Dynamical Model of Wall-Bounded Turbulence

L. Sirovich and X. Zhou
Center for Fluid Mechanics, Brown University, Providence, Rhode Island 02912
(Received 23 December 1992)

Three complex ordinary differential equations, modeling interactions in wall-bounded turbulent flow, are developed and studied. It is believed that the roll-wave interactions which are included are of fundamental importance to turbulence production. Integration of these triad equations is shown to be consistent with direct flow simulations and the Ruelle-Takens route to chaos.

PACS numbers: 47.27.–i

Wall-bounded turbulent flow is characterized by a sequence of events in which a relatively slow moving wall fluid *bursts* [1] into the fast moving core fluid, and the fast moving core fluid *sweeps* [2] into the wall region (see also Ref. [3]). These events, which occur roughly 20% of the time, have an overwhelming effect on force balance at the wall, accounting for roughly 80% of the Reynolds stress at low Reynolds number (Re). Fluctuating turbulent wall flow on average is mainly organized in streamwise counterrotating rolls. (On the basis of *energy*, 75% lie in such modes for low Re [4].) Roll patterns appear as *streaks* in experiments [5]. Theoretical models for their existence have been offered [6,7], but no generally accepted theory exists. The remaining turbulent fluctuations appear as propagating modes which travel downstream at a speed close to the mean speed at the locus of maximal Reynolds stress [4,8]. For channel flow without spanwise constraints propagating modes are plane waves, and have been shown to act as triggers for the *bursts* and *sweeps* of the *streaks* [4,8]. A goal of this Letter is the construction and examination of a simple dynamical model which describes the interaction of key modes and which leads to bursting and sweeping, essential elements of wall-bounded turbulence.

For simplicity, we consider channel flow without spanwise constraint, driven by a constant streamwise pressure gradient, $-k$. If ρ denotes the density of the fluid and H the half channel width, then the friction velocity, $u_*^2 = kH/\rho$, is representative of the rms fluctuations in the wall region. The wall scale is $l_* = \nu/u_*$, and the Kolmogorov scale is roughly $5l_*$ in the sublayer. Experiment [5] and simulation indicate that streaks are of a distribution of roll modes and with peak wavelength close to $100l_*$. (Extension to the turbulent boundary layer requires a slow streamwise dependence in u_* and l_*.) Integration of the mean flow equations yields

$$U = \frac{1}{2}x_2\left(2 - \frac{x_2}{R_*}\right) + \int_0^{x_2/R_*} \overline{u_1 u_2}\, dx_2. \qquad (1)$$

Here and in the following we use the subscripts (1,2,3) to denote the streamwise, wall normal, and spanwise directions and U is the mean flow (streamwise). All velocities are normalized by u_* and length scales by l_*, so that the Reynolds number is $R_* = u_* H/\nu = H/l_*$. The bar signifies the *ensemble average* obtained by averaging over the (x_1, x_3) plane. Velocity fluctuations are incompressible, $\nabla \cdot \mathbf{u} = 0$ and satisfy

$$\frac{\partial}{\partial t}u_i + U\frac{\partial}{\partial x_1}u_i + \delta_{i1}\left(u_2\frac{dU}{dx_2} - \frac{d}{dx_2}\overline{u_1 u_2}\right) + u_{i,j}u_j + \frac{\partial p}{\partial x_i} - \nabla^2 u_i = 0. \qquad (2)$$

p has been normalized by ρu_*^2 and time by $l_*/u_* = \nu/u_*^2$.

Sreenivasan [7] has proposed that, in analogy with transition, the locus of maximal Reynolds stress plays a central role in wall turbulence. Confirmation of this assertion is to be found in the simulations of Sirovich *et al.* [4,8]. As shown there the flow can be optimally represented as a superposition of velocity modes each having the form

$$a^q_{mn}(t)\psi^q_{mn}(x_2)\exp\left[\frac{2\pi i m}{L}(x_1 - Vt) + \frac{2\pi i L}{W}n_3 x_3\right] = a^q_m(t)\exp\left[-\omega_m t\right]\mathbf{V}^q_{mn}(\mathbf{x}). \qquad (3)$$

In simulations, L and W are the periodic length and width of the channel. For relatively low q, V to a good approximation is the mean velocity at the locus of maximal stress. The spatial part dependence in (3) are eigenfunctions of the two point correlation operator. m and n will be referred to as streamwise and spanwise wave numbers and q as the vertical quantum number. The vertical dependence $\psi^q_{mn}(x_2)$ is obtained from simulations [9], and in particular is discussed in Ref. [10]. $a^q_{mn}(t)$ is found to exhibit chaotic behavior typical of turbulence.

We will use the results of simulations in a nominal way to construct a simple physical model. We consider mode energies $\lambda^q_{mn} = \langle |a^q_{mn}|^2 \rangle$ (brackets indicate the time average), the first fifteen of which are [4]

(0,3,1)	(0,1,1)	(0,4,1)	(0,5,1)	(0,4,2)	(0,1,2)	(0,3,2)	(0,2,1)	(0,2,2)	(0,6,1)	(0,5,2)	(1,3,1)	(1,2,1)	(1,4,1)	(1,5,1)
0.0428	0.0399	0.0327	0.0287	0.0229	0.0210	0.0206	0.0197	0.0188	0.0138	0.0131	0.0125	0.0095	0.0084	0.0083

0031-9007/94/72(3)/340(4)$06.00

The first line gives (m,n,q) and the second the percent of total energy in each mode. One must also consider degeneracies based on flow symmetries, e.g., (0,4,1) and (0,−4, 1) have the same energy, as do (1,2,1), $(-1,2,1)$, $(1-2,1)$, and $(-1,-2,1)$. One member of a degenerate set will be used to represent all members of the (invariant) subspace. The energy in the table is the fraction of the total for the subspace.

The most energetic modes are $m=0$ modes (rolls); $q=1$ modes are more energetic than other quantum numbers, and $m=2$ modes are less energetic than the $m=1$ modes. Perturbations based only on roll modes ($m=0$) can be rigorously shown to decay to Poiseuille flow [11]. A model [12] which is based on just such modes has been shown to lead to artifactual behavior [3].

$\mathbf{V}^q_{mn}(\mathbf{x})$ by construction satisfies continuity and hence any finite sum of such terms satisfies continuity. The pressure gradient is orthogonal to the space of such terms and need not be considered. The principal interaction term in (2) is quadratic, *conservative*, and governs the passage of energy among modes. In a Galerkin projection, the quadratic terms lead to triad interactions. For example, to follow the (0,4,1) roll, a possible triad interaction is (0,4,1) ⊗ (1,2,1) ⊗ (1,2,1). (Other possible interactions are considered later.) To follow these modes the flow is assumed to have the form

$$\mathbf{u} \approx A_1\mathbf{V}_{0\,4} + A_2\mathbf{V}_{1\,2} + A_3\mathbf{V}_{1-2} + \text{c.c.}, \tag{4}$$

where for simplicity we have left out the (quantum) $q=1$ dependence. The complex coefficients A_n are time dependent, and it remains to verify that these have secular temporal growth as in (3). If (4) is substituted into (2), then under Galerkin projection we obtain

$$\dot{A}_1 = l_1A_1 - q_1\bar{A}_2A_3 - A_1[c_{11}|A_1|^2 + c_{12}(|A_2|^2+|A_3|^2)], \tag{5}$$

$$\dot{A}_2 = l_2A_2 + q_2\bar{A}_1A_3 - A_2[c_{21}|A_1|^2 + c_{22}(|A_2|^2+|A_3|^2)], \tag{6}$$

$$\dot{A}_3 = l_2A_3 + q_2A_1A_2 - A_3[c_{21}|A_1|^2 + c_{22}(|A_2|^3+|A_3|^2)], \tag{7}$$

where [10] $l_1 = 19.91r - 1.640e/r$, $l_2 = (13.81 - i17.82)r - 0.605e/r$; $q_1 = 0.910$, $q_2 = 1.914 - i1.612$; $c_{11} = 16.56r$, $c_{12} = 10.59r$, $c_{21} = (10.59 - i12.58)r$; $c_{22} = (8.582 - i6.743)r$. Here $r = R_*/R_c$. $R_c = 180$ is the Reynolds number at which $\mathbf{V}_{kl}(x_2)$ were computed and the *eddy viscosity* e is chosen to be 2.7. Cubic terms arise from $\overline{uv}$ in (1).

(5)–(7) have the form of a three-wave resonance. Such equations appear in wave interactions in shear flows [13], in plasmas [14], and in thermal convection to describe roll-hexagon competition [15]. Related equations without cubic terms appear in the interaction between oblique Tollmien-Schlichting (TS) waves and Taylor-Görtler vortices in curved channel flows [16].

Symmetries in the flow confer invariances on the dynamical system. Translational invariance in the streamwise and spanwise directions generates the trigonometric terms in $\mathbf{V}_{0\,4}, \mathbf{V}_{1\,2}, \mathbf{V}_{-1\,2}$. In addition, (5)–(7) are invariant under the group $A_1 \to A_1e^{2ai}$, $A_2 \to A_2e^{(b-a)i}$, $A_3 \to A_3e^{(b+a)i}$, where a, b are arbitrary real constants. The flow geometry possesses a number of reflectional symmetries [17] and from these (5)–(7) are invariant under $A_1 \to \bar{A}_1$, $A_2 \to A_3$, $A_3 \to A_2$. From Lie theory [18] each invariance can reduce the order of the system by one.

To carry out this reduction we use the polar representation, $A_j = r_je^{i\theta_j}$, $i=1,2,3$, which yields

$$\begin{aligned}\dot{r}_1 &= l_1r_1 - q_1r_2r_3\cos\psi - r_1[c_{11}r_1^2 + c_{12}(r_2^2+r_3^2)],\\ \dot{r}_2 &= l_2^rr_2 + qr_1r_3\cos(\psi+\theta_0) - r_2R_2^r,\\ \dot{r}_3 &= l_2^rr_3 + qr_1r_2\cos(\psi-\theta_0) - r_3R_2^r,\end{aligned} \tag{8}$$

$$\dot{\theta}_1 = -q_1\frac{r_2r_3}{r_1}\sin\psi, \quad \dot{\theta}_2 = l_2^i + q\frac{r_1r_3}{r_2}\sin(\psi+\theta_0) - R_2^i,$$
$$\dot{\theta}_3 = l_2^i - q\frac{r_1r_2}{r_3}\sin(\psi-\theta_0) - R_2^i, \tag{9}$$

where $\psi = \theta_3 - \theta_2 - \theta_1$, $R_2^r = c_{21}^rr_1^2 + c_{22}^r(r_2^2+r_3^2)$, $R_2^i = c_{21}^ir_1^2 + c_{22}^i(r_2^2+r_3^2)$, $qe^{i\theta_0} = q_2$, and c_{2j}^r, c_{2j}^i are the real and imaginary parts of c_{2j} with $j=1,2$. The three equations of (9) can be reduced to

$$\dot{\psi} = q\frac{r_2r_3}{r_1}\sin\psi - q\frac{r_1r_3}{r_2}\sin(\psi+\theta_0) - q\frac{r_1r_2}{r_3}\sin(\psi-\theta_0). \tag{10}$$

(5)–(7) can be reduced to (8) and (10), in the variables r_1, r_2, r_3, and ψ.

Other possible interactions: Possible triads which can enter in the evolution of the (0,4,1) mode are (0,4,1) ⊗ (0,2,1) ⊗ (0,2,1) and (0,4,1) ⊗ (0,1,1) ⊗ (0,3,1), which are pure roll mode interactions. By themselves such interactions cause relaminarization to Poiseuille flow and take place at a slow pace [4,8], and are not significant to the rapid dynamics of wall turbulence. Another possible triad interaction is (0,4,1) ⊗ (1,3,1) ⊗ (1,1,1). This may be neglected since (1,1,1) (which does not appear in the table) is at a lower energy so the interaction is weak. Also in the evolutionary equation for $a_{04}^{(1)}$ (i.e., for A_1) this interaction leads, e.g., to a term $\propto a_{13}^1a_{-11}^1$, but the product is uncorrelated $\langle a_{13}a_{-11}\rangle = 0$ in the exact interaction which is further evidence that this is weak.

To test such ideas we integrated the (0,3,1) ⊗ (1,5,1) ⊗ (1,2,1) triad along with (5)–(7) and coupled through (1,2,1) to (5)–(7) to numerical integration and found that (0,3,1) and (1,5,1) decayed to zero under normal initial conditions. Similarly (0,6,1) ⊗ (1,3,1) ⊗ (1,3,1) is an eligible triad of the table, and is coupled to (5)–(7) through cubic terms; e.g., $A_{04}|A_{13}|^2$ appears in (5)–(7). If these coupled triads are numerically integrated, the modes in the second triad decay to zero. [If (0,6,1) ⊗ (1,3,1) ⊗ (1,3,1) is decoupled it supports nonzero solutions, which, however, are nonchaotic at the relatively low Re we consider.] Other numerical experiments further support the idea that the triads interact weakly. We regard (5)–(7)

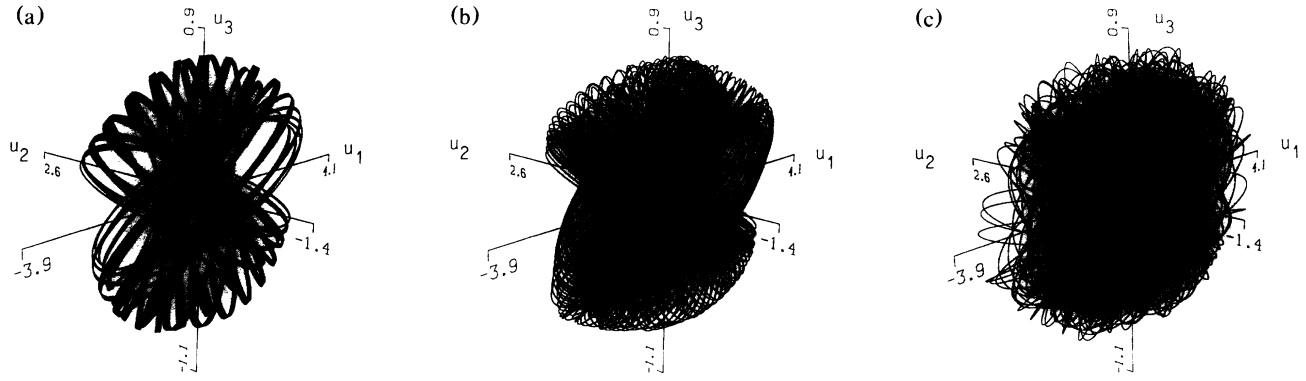

FIG. 1. Three-space of the fluid velocity. (a) $R_* = 156$, (b) $R_* = 158.4$, and (c) $R_* = 168$.

as being representative and now discuss their solutions.

Steady solutions: (A) $A_1 = A_2 = A_3 = 0$, corresponding to plane Poiseuille flow, is stable if $l_1, l_2^r < 0$ or if $R_* < 62.2$. Coincidentally, this is the value of R_* found in simulations and experiments [19]. (B): $|A_1|^2 = l_1/c_{11}, A_2 = A_3 = 0$. The condition that $l_1 > 0$ implies that $R_* > 84.9$. Physically this solution corresponds to one steady roll in the flow, which may be shown to be unstable.

Periodic solutions: (A) $A_1 = 0$, $A_2 = 0$, $A_3 = ae^{i\omega t}$ with $a = \sqrt{l_2^r/c_{22}^r}$, $\omega = l_2^i - c_{22}^i a^2$, a single oblique wave. By symmetry, $A_2 = ae^{i\omega t}$, and $A_1 = A_3 = 0$ is also a solution. It may be shown that for $62.2 < R_* < 130.7$, both of these solutions are stable, and which solution appears depends on the initial conditions. (B) Another periodic solution can be found by letting $A_1 = r_{10}$, $A_2 = r_{20}e^{i\omega t}$, $A_3 = \pm A_2$; here r_{10} and r_{20} are real, determined by $l_1 r_{10} \mp q_1 r_{20}^2 - r_{10}(c_{11}r_{10}^2 + 2c_{12}r_{20}^2) = 0$, $l_2^r \pm q_r r_{10} - (c_{21}^r r_{10}^2 + 2c_{22}^r r_{20}^2) = 0$ and the frequency by $\omega = l_2^i \pm q_i r_{10} - (c_{21}^i r_{10}^2 + c_{22}^i r_{20}^2)$, with $q_r = \mathrm{Re}(q_2)$, $q_i = \mathrm{Im}(q_2)$. This solution corresponds to two oblique waves and one steady roll. The stability can be investigated by means of the polar decomposition, (8) and (10). A 4×4 Jacobi matrix obtained at $r_1 = r_{10}$, $r_2 = r_{20}$, $r_3 = r_{20}$, $\psi = 0, \pi$ determines the eigenvalues which in turn determine the stability. From this it is found that the solution is always unstable whenever it exists. This result is consistent with a simulation in which the flow field evolving from a pair of oblique waves is characterized by a rapid development into a turbulentlike state [20].

Quasiperiodic and chaotic solutions: For $130.7 < R_* < 157.5$, we find *simple* quasiperiodic solutions, with $A_1(t)$, $r_2(t)$, and $r_3(t)$ periodic and $A_2 = r_2(t)e^{i(\omega t+\beta)}$, $A_3 = r_3(t)e^{i(\omega t+\alpha)}$ quasiperiodic because of the appearance of the second frequency ω. When $157.5 < R_* < 166$, we find *complicated* quasiperiodic solutions, meaning that $A_1(t)$ is no longer periodic. The solutions appear complicated but some symmetries are preserved. In the interval $166 \leq R_* < 180$, chaos and quasiperiodic solutions coexist.

In order to view the flow of these solutions in phase space we consider the three space of the fluid velocity itself (u, u_2, u_3) at some nominal location in space. Figure 1 depicts this behavior at three representative values of the control parameter R_*. In the range $130.7 < R_* < 157.5$ the motion lies on a two-torus and this is seen in Fig. 1(a). (This was calculated at Re= 156.) In the range $157.5 < R_* < 166$ the motion lies on a three-torus. The orderliness of this motion is shown in Fig. 1(b) (calculated at $R_* = 158.4$). A typical example (drawn for $R_* = 168$) of the chaotic range $166 < R_* < 180$ is

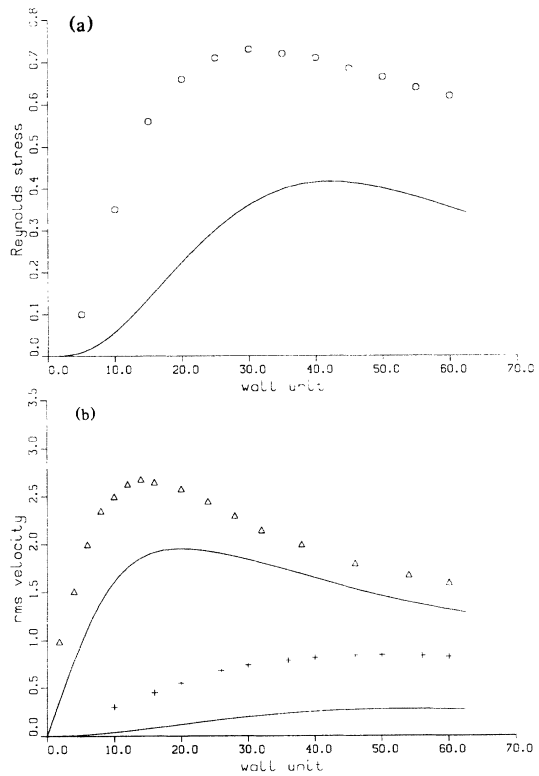

FIG. 2. A comparison of the statistics with the full simulation; data from the original simulation are marked; the solid lines are from the model equations at $R_* = 180$. (a) Average Reynolds stress $-\overline{uv}$; (b) root mean square velocity of streamwise component u_{rms} and normal component v_{rms}.

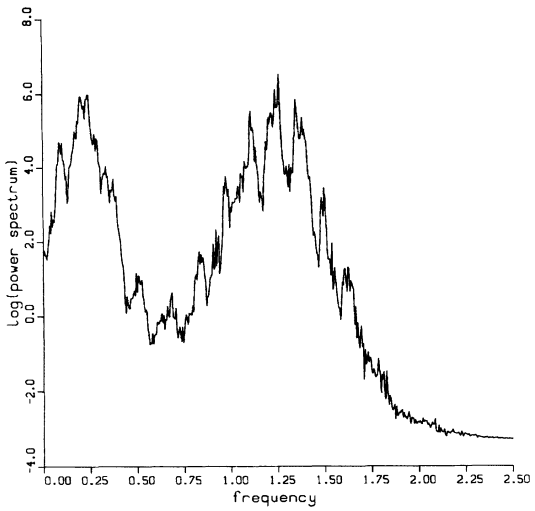

FIG. 3. The power spectrum at $R_* = 180$.

shown in Fig. 1(c). For special, nongeneric initial data quasiperiodic trajectories may also be found in this range. Although three-torus motion appears, it is not typical. The likely route to chaos follows the Ruelle-Takens scenario [21] in which three-torus motion experiences a symmetry breaking. This is in contrast with the heteroclinic cycle which is central to earlier models [12] and which is very likely an artifact of Galerkin projection [22].

The chaos which is found in this simple model shares a number of features found in large scale turbulent simulations. The amplitude and phase of propagating modes closely resembles typical curves found in the full simulation [4], and thus the propagation property is verifed. The components of $(\mathbf{u})_{\mathrm{rms}}$ and average Reynolds stress for the model are shown in Fig. 2 and although these are quantitatively different from what is found in the full simulation [4], the qualitative resemblance is striking. The temporal power spectrum shown in Fig. 3 also closely resembles that found in a more complicated model [10] and shows a second peak as indicated in recent experiments [23].

Real turbulence occurs as the result of countless interactions among roll-like and wavelike modes [4]. In the present investigations we have demonstrated a range of behavior for the basic triad interactions. This model is of a stereotypical type and captures fundamental features of wall-bounded turbulent flows. In a full simulation or a real experiment such triads may be regarded as interacting subsystems. Moreover, as we have argued in a limited sense these interactions appear to be relatively weak. If the table is expanded to include more modes, the interactions become more complex. Within a limited framework of computation we have shown that the interactions are relatively weak. We regard our model as a *caricature* or as being *impressionistic* [24]. Furthermore, it is a speculation that wall-bounded turbulence may be described by a (Re dependent) system of weakly interacting triads.

This work was supported by NSF (No. IRI-911645), Ormat Industries, and Pittsburgh Supercomputing Center.

[1] S.J. Kline, W.C. Reynolds. F.A. Schraub, and P.W. Rundstadler, J. Fluid Mech. **30**, 741 (1967).
[2] E.R. Corino and R.S. Brodkey, J. Fluid Mech. **37**, 1 (1969).
[3] W.W. Wilmarth, Adv. Appl. Mech. **15**, 159 (1975); Annu. Rev. Fluid Mech. **7**, 13 (1975); J.P. Kim, P. Moin, and R.D. Moser, J. Fluid Mech. **177**, 133 (1987).
[4] L. Sirovich, K.S. Ball, and R.A. Handler, Theor. Comput. Fluid Dyn. **2**, 307–317 (1991).
[5] H.T. Kim, S.J. Kline, and W.C. Reynolds, J. Fluid Mech. **50**, 133 (1971).
[6] P.S. Jang, D.J. Benny, and R.L. Gran, J. Fluid Mech. **169**, 109 (1986).
[7] K.R. Sreenivasan, in *Turbulence Management and Relaminarization*, edited by H.W. Liepmann and R. Narasimha (IUTAM, 1987).
[8] L. Sirovich, K.S. Ball, and L.R. Keefe, Phys. Fluids A **2**, 2217–2226 (1990).
[9] P. Moin and R.D. Moser, J. Fluid Mech. **200**, 471 (1988).
[10] X. Zhou and L. Sirovich, Phys. Fluids A **4**, 2855 (1992).
[11] H.K. Moffatt, in *Whither Turbulence?* edited by J. L. Lumley (Springer-Verlag, Berlin, 1990), pp. 250–257.
[12] N. Aubry, P. Holmes, J.L. Lumley, and E. Stone, J. Fluid Mech. **192**, 115 (1988); also see S. Sanghi and N. Aubry, J. Fluid Mech. **247**, 455 (1993); N. Aubry and S. Sanghi, in *Chaotic Dynamics in Fluid Mechanics*, edited by K.N. Ghia and V. Ghia (ASME, New York, 1989).
[13] A.D.D. Craik, Proc. R. Soc. London A **343**, 351 (1975).
[14] J. Weiland and H. Wilhelmsson, *Coherent Nonlinear Interaction of Waves in Plasmas* (Pergamon, Oxford, 1977).
[15] L.A. Segel, J. Fluid Mech. **21**, 359 (1965); S. Ciliberto, P. Coullet, J. Lega, E. Pamaloni, and C. Perez-Garcia, Phys. Rev. Lett. **65**, 2370 (1990).
[16] P. Hall and F.T. Smith, Proc. R. Soc. London A **417**, 255 (1988).
[17] L. Sirovich, Q. Appl. Math. **XLV**, No. 3, 561 (1987). See also M. Dellnitz, M. Golubitsky, and M. Nicol, in *Trends and Perspectives in Applied Mathematics*, edited by L. Sirovich (Springer-Verlag, Berlin, 1994).
[18] G. Blumen and J. Cole, *Similarity Methods for Ordinary Differential Equations* (Springer-Verlag, Berlin, 1974).
[19] K.S. Ball, K.S. Watson, and R.A. Handler, Bull. Am. Phys. Soc. **37**, 1751 (1992); V.C. Patel and M.R. Head, J. Fluid Mech. **38**, 181 (1969).
[20] P.S. Schmid and D.S. Henningson, Phys. Fluids A **4**, 1986 (1992).
[21] S. Newhouse, D. Ruelle, and F. Takens, Commun. Math. Phys. **64**, 35 (1978).
[22] L. Sirovich and X. Zhou, Phys. Fluids A (to be published); also see G. Berkooz, P. Holmes, J. Lumley, N. Aubry, and E. Stone, Phys. Fluids A (to be published).
[23] K. Ball, D.G. Bogard, and C. Gan (private communication).
[24] R. Narishima, in *Whither Turbulence?* (Ref. [11]), pp. 13–48.

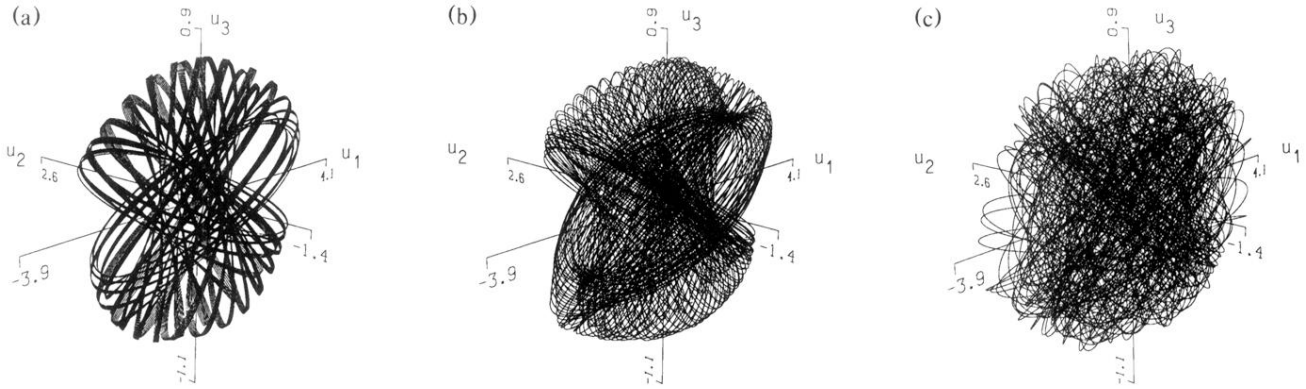

FIG. 1. Three-space of the fluid velocity. (a) $R_* = 156$, (b) $R_* = 158.4$, and (c) $R_* = 168$.